Soft Matter

Accepted Manuscript

ROYAL SOCIETY OF CHEMISTRY

www.rsc.org/softmatter

ARTICLE TYPE www. rsc.org/xxxxxx | XXXXXXXX

In-plane particle counting at contact lines of evaporating colloidal drops: effect of the particle electric charge†

Diego Noguera-Marín,[a] Carmen L. Moraila-Martínez,[a] Miguel A. Cabrerizo-Vílchez,[a] and Miguel A. Rodríguez-Valverde*[a]

Received Xth XXXXXXXXXX 20XX, Accepted Xth XXXXXXXXX 20XX
First published on the web Xth XXXXXXXXXX 200X
DOI: 10.1039/b000000x

Complete understanding of colloidal assembly is still a goal to be reached. In convective assembly deposition, the concentration gradients developed in evaporating drops or reservoirs are usually significant. However, collective diffusion of charge-stabilized particles has been barely explored. The balance between convective and diffusive flows may dictate the particle dynamics inside evaporating colloidal drops. In this work we performed in situ counting of fluorescent particles in the vicinity of the triple line of evaporating sessile drops by using Confocal Laser Scanning Microscopy. We used particles of different size, with different charge response over the pH scale and we focused on charged and nearly uncharged particles. Two substrates with different receding contact angle were used. Binary colloidal mixtures were used to illustrate simultaneously the accumulation of particles with two different charge states at the triple line. The deposition rate close to the triple line was different depending on the electric state of the particle, regardless of the substrate used.

1 Introduction

Convective/capillary self-assembly is a rising topic due to its multiple applications[1–4]. Colloidal assembly inside a sessile drop is ruled by the so-called "coffee ring" effect[5]. During the evaporation of a sessile drop, due to its curved geometry[6], a surface gradient of the local evaporation rate is established leading to a faster evaporation at the three-phase contact line. To balance this liquid loss, a convective flow is originated inside the drop towards the triple line. Full description of the velocity field associated to this flow is a non trivial task because velocity depends on time, position and receding contact angle[7]. The latter dependance states that lower receding contact angles produce higher convective flows[8].

As particles accumulate close to the contact line, a concentration gradient will occur inside the evaporating drop and, to counteract it, particle diffusion should develop an inward counterbalancing flow following the Fick's law. Collective diffusion in dense systems depends on hydrodynamic and many-body direct interactions[9]. It is known that the collective diffusion coefficient diverges as the concentration is close to the maximum packing fraction[10,11]. This increase is much greater for charged particles than for uncharged particles[12]. In this scenario, convective/capillary deposition of charged particles may be regarded as a competition between two opposing flows: convective and diffusive flows[13–15]. This balance between flows might dictate the particle dynamics inside the evaporating drop.

Collective diffusion of charged particles in convective assembly deposition has been barely explored[12]. Experimental results on the dynamics of charge-stabilized colloids at high concentrations are very scarce. Besides, in the complex evaporating process, it is difficult to distinguish diffusive and convective displacements of particles by imaging techniques. Although other techniques might be used to measure collective diffusion such as dynamic light scattering and pulsed field gradient NMR, in-situ measurements of concentration profiles are hardly realizable. Otherwise, fluorescent particles have been successfully used to record dynamics inside colloidal drops in the vicinity of the contact line.[16,17] Confocal Laser Scanning Microscopy (CLSM) is a well-established technique[18] that allows real time imaging of fluorescent targets. Since a mixture of charged and non-charged particles can segregate based on differing diffusion rates[19], the use of bidisperse suspensions and CLSM would allow to illustrate simultaneously the accumulation of two different particles at the triple line.

The aim of this work is to examine the role of the particle electric charge in convection-driven self-assembly. In this

† Electronic Supplementary Information (ESI) available: Pdf document with Figure S1: Electrophoretic mobility of glass (40nm, 0.01% (w/w), AttendBio) and PMMA nanoparticles (110nm, 0.01% (w/w), Microparticles) in terms of pH. Pdf document with Figure S2: Sequence of images of negatively charged MF-l particles at pH12 and 0.01% (w/w) over a PMMA substrate. The objective used was 40X to visualize a greater area for illustrative purposes. The accumulation of particles at the fixed contact line is clear (a-c). After 490s, the triple line began to recede (d) and it transported the charged particles. Several isolated deposits (e-h) were formed due to local pinning of the contact line.

[a] *Biocolloid and Fluid Physics Group, Applied Physics Department, Faculty of Sciences, University of Granada, E-18071 Granada (Spain). Fax: +34 95824 3214; Tel: +34 95824 3229; E-mail: marodri@ugr.es*

work we performed in-plane counting of fluorescent particles in the vicinity of the triple line of evaporating drops by using CLSM. For the same evaporation conditions, fluorescent-labeled particles with different charge-response over the pH scale were studied. Size, concentration and electric charge of the particles were conveniently selected accordingly. The use of two substrates with different receding contact angle allowed to explore different evaporation convective flows.

2 Materials and methods

2.1 Substrates

We used glass microscope coverslips (0.1mm-thick, 60x24 mm^2, Thermo Scientific) and polymethyl-metacrylate sheets (PMMA, 0.05mm-thick, Goodfellow) as substrates. These substrates were selected because of their transparency, smoothness and small thickness. The glass coverslips were conveniently cut with a diamond tip. On the other hand, due to the bending of the thin PMMA sheets, we designed a titanium holder (64x26mm^2) with a circular hole of 1cm diameter at its center. This way, the PMMA substrate was not deformed by the immersion objective of the confocal microscope. Before each experiment, the PMMA substrates were cleaned by ultrasonic rinsing in a detergent solution (Micro90) during 10min and next in Milli-Q water (20min). The glass substrates were sonicated in the same detergent solution (15min), next in 70% (v/v) acetone (15min), then in 70% (v/v) ethanol (15min) and finally in Milli-Q water (30min).

The wettability properties of the substrates were studied using the captive bubble technique[20]. It is worth to notice that the water receding contact angle of the substrates did not depend on the pH value. The results for the advancing and receding contact angles are shown in Table 1. The electric behavior over the pH scale was estimated qualitatively by measuring the electrophoretic mobility of nanoparticles composed of the same material as the substrates (see Figure S1 in supplementary data). Over the entire pH range the substrates were negatively charged although with different magnitude. We measured the roughness of the substrates using a white light confocal microscope (PLμ, Sensofar Tech S.L.). The root mean square roughness measured over 210x285μm^2 was 28.2 nm for the glass substrate and 24.4 nm for the PMMA substrate.

Substrate	θ_A (°)	θ_R (°)
Glass	16 ± 4	10 ± 3
PMMA	93 ± 1	62 ± 1

Table 1 Results of advancing and receding contact angle measured with the captive bubble technique for the substrates studied in this work.

2.2 Particle suspensions

We purchased aqueous suspensions of Melamine-Formaldehyde (MF) particles labeled with two different fluorochromes (Rhodamine-B and Fluorescein Isothiocyanate) and Rhodamine-B labelled carboxylated-MF particles. The particles were supplied by Microparticles at ϕ_m =2.5% (w/w). In Table 2 we summarize the properties of the particles used.

The MF and MF-COOH particles have a pH-dependent surface charge due to their terminal polar groups. To change the electrostatic double layer interactions between particles, we varied the particle electric charge through the medium pH[21]. The particles were diluted in buffered solutions of low ionic strength ($\leq$15mM). We used a Zetasizer Nano device (Malvern, 4mW He-Ne laser, 633nm wavelength) to measure the electrophoretic mobility of the particles. The weight fraction used for these measurements was ϕ_m=0.01%. From Figure 1, we observe that the MF and MF-COOH particles have different isoelectric points. From the corresponding isoelectric points, we selected two pH values for each particle to explore two different electric states: pH10 and pH12 where the MF particles were nearly uncharged and charged, respectively and pH4 and pH10 where the MF-COOH particles were nearly uncharged and charged (see Figure 1). Binary mixtures of MF-l and MF-COOH particles, with different fluorochrome but similar size, were prepared at pH4 and pH10 with a ratio 1:1 in the particle number. Since the possible effects caused by the collective diffusion on the particle deposits can be mostly dampened at high bulk concentrations, we prepared the particle suspensions at very low concentration (0.005-0.01% (w/w)). This way, the concentration gradients developed inside the drop should be significant during the evaporation.

2.3 Experimental set-up

We used CLSM with an inverted microscope (DMI6000, Leica) as described in Figure 2 to analyze the in-plane behavior of the particles transported towards the neighborhood of the contact line. We used a 100X objective over a window of 77.5x77.5 μm^2, and occasionally a 40X objective over 156x156μm^2. The z-depths of field were 0.7 μm and 1.8μm with the 100X and 40X objectives, respectively. These parameters allowed to count only the particles deposited just on the substrate near the contact line. This way, we observed the horizontal particle motion and the sudden showing of some particles, coming from out-of-focus planes. The CLSM device has different lasers (Blue diode of 405 nm, Argon laser [458, 476, 488, 496 and 514 nm] and He/Ne lasers of 543, 594 and 633 nm). We selected the light source depending on the absorbance of each particle (see Table 2). The drop volume was 3μl and the experiments were carried out at $\approx$22-25°C

Particle	Acronym	Fluorochrome	λ_{abs}(nm)	λ_{em}(nm)	Diameter (μm)
Melamine Formaldehyde	MF-s	Rhodamine-B	560	584	0.366±0.06
Melamine Formaldehyde	MF-l	Fluorescein Isothiocyanate	506	529	1.11±0.05
Carboxylated-Melamine Formaldehyde	MF-COOH	Rhodamine B	560	584	1.09±0.07

Table 2 Properties of the fluorescent particles used in this study.

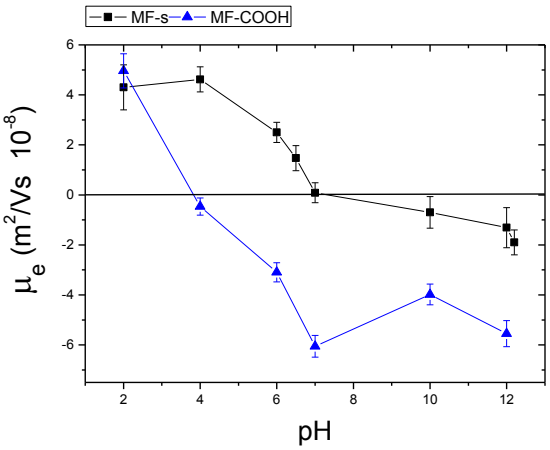

Fig. 1 Electrophoretic mobilities for the MF and MF-COOH particles. All measurements were performed with low ionic strength buffers at 0.01% (w/w).

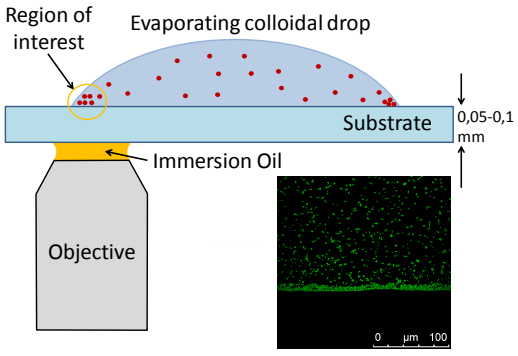

Fig. 2 Set-up used to count the particles arriving at the triple line of an evaporating colloidal drop. The region of interest is reduced to the triple line and its immediate vicinity: a square window of 77.5 or 156 μm side depending on the objective used.

and RH≈38-42%. The images obtained (512x512 pixel) were captured each 1.3s and analyzed with the public software ImageJ. For the particle counting, the number of red or green pixels per frame were counted and divided by the pixels occupied by a single particle. The larger particles were also counted by segmentation[22]. Both procedures acceptably agreed. We evaluated the particle increment in the region of interest, from the beginning of the image acquisition. Next, the particle increment was divided by the drop area visualized in each experiment. The estimation of drop area was the main source of error during the image processing. We reduced our analysis to pinned triple lines. In those experiments where the contact line receded, the particle counting was interrupted because the wet area varied.

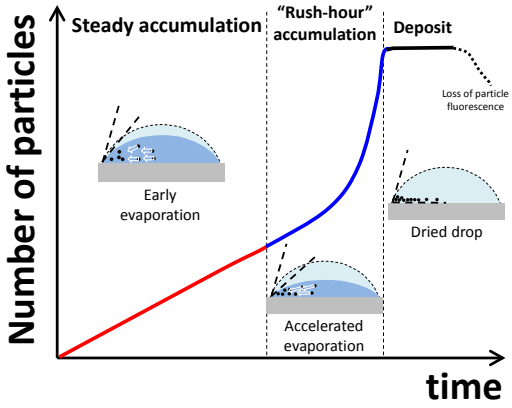

Fig. 3 Typical behavior of the particle increment per unit area in terms of time. Three stages with different slope can be identified: steady accumulation, "rush-hour" accumulation and deposit formation.

In Figure 3 we describe the stages reproduced in a typical plot of increment of particles per wet area in terms of time. There are three recognizable stages with different slope (flow rate). During the early evaporation, with small variations of volume and contact angle, the particles are steadily accumulated at the pinned triple line. The zero time for each plot corresponds to the beginning of the image acquisition after the drop deposition and plane focusing. The time delay was lower than 1 min. When the evaporation accelerates, the contact angle significantly decreases and the convective flow in-

creases. We identify this "rush-hour" effect in the deposition rate[23] with the drop collapse. The "rush-hour" stage can be more or less pronounced according to the experimental conditions and the system characteristics. Finally, once the number of particles accumulated saturates because no more particles are arriving to the fixed triple line, the region of drop analyzed is dried. During this final stage, the particle counting (fluorescence signal) can fluctuate or even decrease due to the dehydration of the particles and proximity between them leading to resolution artifacts. Depending on the contact line dynamics, firstly ruled by the receding contact angle of substrate and the occurrence of self-pinning[5], the overall time of the experiments was different. We measured the particle flow per unit of wet area during the early evaporation with a reproducibility level of 25-40%. The final amount of material deposited (particles/μm^2) was roughly estimated.

3 Results and discussion

In experiments carried out on glass substrates under the same evaporation conditions, we observe that the uncharged particles accumulated at the contact line at faster rate than the charged ones (see Figure 4). This behavior was found regardless of the particle size (see Figures 4-(a) and (b)), the type of particle (see Figures 4-(b) and (c)), and the particle concentration (see Figures 4-(b) and (d)). From the linear behavior of each particle increment, we compared the slopes obtained. The nearly uncharged MF-s particles arrived to the contact line 47.3 times faster than the charged ones, and the ratio between amount of material deposited was 5. At the same solid fraction (ϕ_m=0.01%), the barely charged MF-l particles accumulated 7.4 times faster than the charged MF-l particles due to the lower number of larger particles although the ratio between the masses of final deposit was 6. The uncharged MF-COOH particles, at the same concentration than the MF-l particles and with similar size, accumulated 2.2 times faster than the charged MF-COOH particles and the mass of the final deposit was 3 times greater. The difference between the charged MF-l and MF-COOH particles might be explained by the type of the interparticle interaction potential (surface electric potential, hydration layer, range), which can affect differently the osmotic compressibility of the dispersion and the hydrodynamic interactions. Finally, at lower particle concentration (ϕ_m=0.005%), the deposition of the barely charged MF-l particles was mitigated although it was 2.5 times faster than for the charged MF-l particles and the mass deposited was 1.7 times greater. The rate of deposition of charged particles revealed the particular balance between the outward convective flow and the inward diffusive flow. The interacting particles are transported towards the contact line at the same time while they intend to diffuse away from it, rather than the uncharged particles, due to their greater diffusion coefficient near the contact line. Decreasing the bulk concentration (number of particles), the relative difference between uncharged and charged particles is also reduced because the evaporation-driven convective flow produces lower concentration gradients. Although our measurements were restricted just to the horizontal surface of the substrate, the development of vertical concentration gradients is not discarded.

The accumulation of barely charged particles was also favored on PMMA substrates, rather than with the charged ones, under the same evaporation conditions (see Figure 5). However, the particle deposition was less favored than on the glass substrates by the low convective flow developed on the PMMA substrates due to their higher receding contact angle. This reduced significantly the differences between nearly uncharged and charged particles except for the "rush-hour" stage, where the convective flow became significant as well as the local particle concentration. At ϕ_m=0.01%, the uncharged MF-COOH particles initially arrived at the contact line on the PMMA substrate only 1.5 times faster forming a deposit 2 times greater (see Figure 5-(a)) whereas the uncharged MF-s particles accumulated 1.3 times faster than the charged ones and the final deposit was 1.9 times greater (see Figure 5-(b)). As shown in Figure S2 of supplementary data with charged MF-l particles at ϕ_m=0.01%, the contact line mostly receded on the PMMA substrates with micron-sized particles although the faster accumulation of uncharged particles could delay, or even occasionally frustrate, this receding motion by enhancing the self-pinning. However, by using nanometer-sized particles at the same solid fraction, the triple line remained pinned during the complete evaporation of the drop, regardless of the particle charge. In Figure 5-(b), we also observe a unexpected behaviour of the nearly uncharged MF-s particles. They were transported faster than the charged ones at the beginning of the drop evaporation, but their deposition was suddenly retarded and as consequence there was a greater increment of charged MF-s particles at the triple line. At the time that the drop containing charged MF-s particles collapsed and dried, the nearly uncharged MF-s particles began to describe a marked "rush-hour" motion up to exceed significantly the number of charged MF-s particles accumulated at the contact line at the end of drop evaporation, as shown in Figure 4-(a) on the glass substrate. When we used smaller particles (MF-s) on the PMMA substrate, a much greater number of particles arrived to the contact line despite of the low convective flow. This scenario should enhance the collective diffusion of charged nanoparticles, as happens at short times, but the own arrangement of the uncharged MF-s particles at the contact line could affect the local evaporation rate of the drop and as consequence, the "coffee-ring" effect. Due to the high receding contact angle of the PMMA substrate, the plausible piling up of particles inside the interfacial "wedge" of the drop and the resulting adsorption at the water-air interface (skin formation) might explain

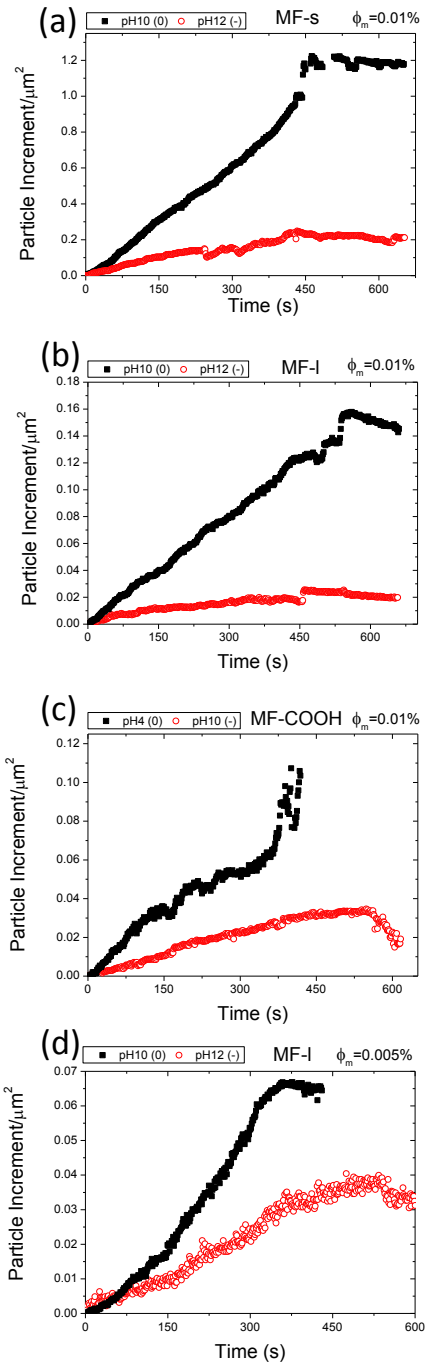

Fig. 4 Number increment of particles per unit of drop area with different size, nature and concentration deposited on glass substrates for two electric states. The particles used were: (a) MF-s at 0.01% (w/w), (b) MF-l at 0.01% (w/w), (c) MF-COOH at 0.01% (w/w) and (d) MF-l at 0.005% (w/w).

both the slower drop evaporation and the late avalanche-like outward motion of the barely charged nanoparticles. On the glass substrate, this effect was not found because the small "wedge" enabled the formation of a particulate film[24] rather than the particle piling up and besides the strong evaporative flux was hardly decreased.

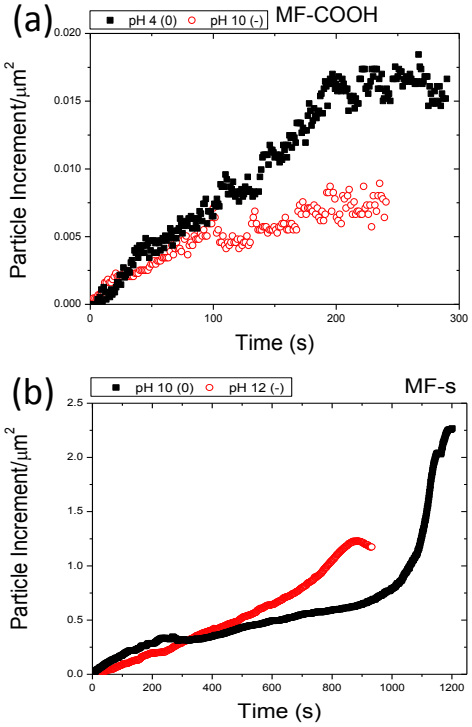

Fig. 5 Particle increment per unit of drop area obtained on PMMA substrates for different charge states of (a) the MF-COOH particles and (b) the MF-s particles at 0.01% (w/w).

We further conducted experiments with 1:1 binary mixtures of the MF-l and MF-COOH particles at ϕ_m=0.01% (0.005% of each particle) on glass substrates. Although the bulk concentration and size was the same for both particles, the collective diffusion coefficient was expected to be different[19]. At pH4, the MF-COOH particles were nearly uncharged while the MF-l particles were positively charged and at pH10, the MF-l particles were nearly uncharged while the MF-COOH particles were negatively charged (see Figure 1). Figure 6 shows the number increment of particle for the two bi-disperse suspensions. The rate of accumulation of the nearly uncharged MF-l particles was 4.9 times greater than the negatively charged MF-COOH particles whereas the final amount of material deposited 3.9 times greater (see Figure 6-(a)). In Figure 6-(b), the rate of accumulation during the initial evaporation was identical for both particles. However, during the "rush-hour" stage, the increment of the barely charged MF-

COOH particles overcomes the positively charged MF-l particles. It is important to take into account that these MF-l particles moving close to the negatively charged substrate should be further pushed towards it. Unlike the negatively charged particles, the positively charged particles are transported by three different mechanisms: the outward convective flow, the electrostatic attraction and the inward diffusive flow. This way, the identical early behaviour of the MF-l and MF-COOH particles can be explained once the collective diffusion and substrate-particle attraction were mutually cancelled. However, during the "rush-hour" stage, the gradient of particle concentration was high enough so that the particle diffusion overcame the electrostatic interaction and mitigated the arrival of charged MF-l particles. This result points out to that the effect of the electrostatic substrate-particle interaction, even when the substrate and the particle are mutually attracted, is weaker on the final deposition than the electrostatic particle-particle interaction.

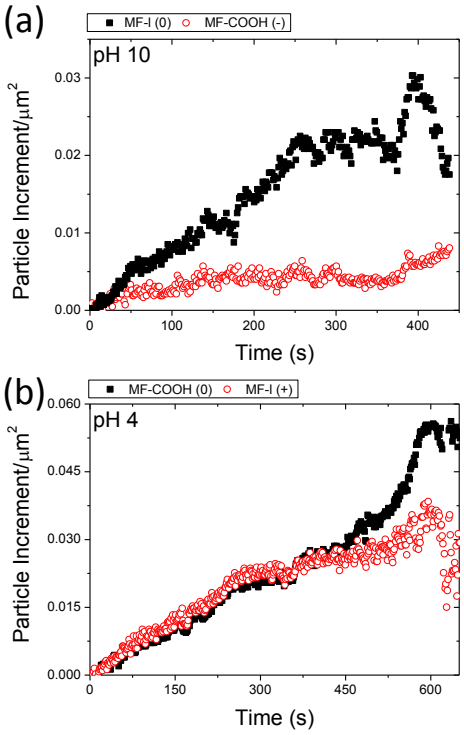

Fig. 6 Particle increment per unit of drop area obtained with bi-disperse suspensions on glass substrates. The suspensions were prepared at 0.01% (w/w), 1:1 in number of particles and with different charge states: (a) nearly uncharged MF-l and negatively charged MF-COOH particles (pH 10), (b) nearly uncharged MF-COOH and positively charged MF-l particles (pH4).

In binary mixtures, it is important to take into account that certain competing effects were present. Hydrodynamic and

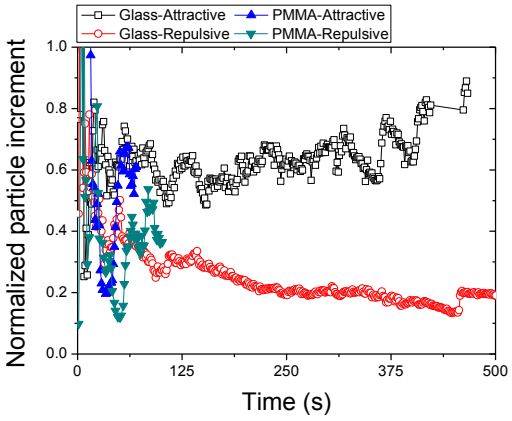

Fig. 7 Normalized number increment of the charged MF-l particles at 0.01% (w/w) over the glass and PMMA substrates for different substrate-particle interaction. The increment per unit of wet area of the charged particles was divided by the increment per unit of wet area of the nearly uncharged particles, under the same evaporation conditions.

direct interactions might affect the osmotic pressure in a different manner than in a monodisperse suspension prepared at the same concentration. For this purpose, we compared Figure 6-(a) with experiments carried out under the same conditions but with the corresponding monodisperse suspensions (not shown). The relative rate of accumulation between nearly uncharged MF-l and negatively charged MF-COOH particles was greater in binary mixtures (4.9 times) than in separate monodisperse suspensions (2.8 times). Despite these effects, the role of the particle electric charge proved to be significant for the particles arriving at the triple line.

Finally, we explored the substrate-particle interaction. Three experiments were performed with the MF-l particles at ϕ_m=0.01% on the glass and PMMA substrates: 1) negatively charged particles (substrate-particle repulsion), 2) positively charged particles (substrate-particle attraction) and 3) nearly uncharged particles (no significant interaction with the substrates). Results are summarized in Figure 7. We normalized the increment of charged particles arriving at the triple line per unit of wet area by the corresponding increment of uncharged particles, under the same evaporation conditions. From the values of contact angle hysteresis and receding contact angle, the drop evaporation on the PMMA substrate took longer than on the glass substrate. However, the experiment time was longer with the glass substrates because the triple line remained pinned until the complete evaporation. Whereas, for the PMMA substrates, the particle counting was interrupted when the contact line started to recede. Although, electrostatic attraction between particle and substrate enhances the deposition, it can be observed that all data are lower than

the unit regardless of the type of substrate-particle interaction. This reveals that the positively and negatively charged particles are alike transported towards the contact line at a slower rate than the nearly uncharged particles, regardless of the substrate used. The balance between diffusive and convective flows seems to overcome the interaction between particle and substrate.

4 Conclusions

By using fluorescence confocal microscopy, we monitored the in-plane particle accumulation close to the contact line during drop evaporation. We found that collective diffusion mitigated the arrival of charged particles to the contact line, regardless of the type of particle and substrate used. The barely charged particles accumulated at the contact line from 40 up to 1.3 times faster than the charged particles, according to the case (concentration, particle size, type of substrate).The experiments carried out with binary colloidal mixtures plainly illustrate the influence of collective diffusion on the particle deposition. This opens up a new route in convective/capillary self-assembly for the particle segregation ruled by electric charge. These results may serve as a basis for the development of advanced theoretical models that describe the transport of the colloidal particles with the full convection-diffusion equation. In this scenario, substrate-particle electrostatic repulsion has no significant effect because, even for unlike charged substrate-particle systems (preferential deposition), the deposition was more favored with uncharged particles than with charged ones. However, the substrate does modulate the particle increment close to the contact line through the evaporation-driven capillary flow. The deposition of charged and nearly uncharged particles at short times is significantly different on substrates with small receding contact angles (high convective flows). The substrate wettability properties and particle deposition are coupled because self-pinning affects contact line dynamics, and the particle accumulation depends at different extent on the space available near the contact line, the time of natural pinning and mostly, the convective flow.

Acknowledgements

This work was supported by the "Ministerio Español de Ciencia e Innovación" (project MAT2011-23339) and the "Junta de Andalucía" (project P12-FQM-1443). D. Noguera thanks to the Biocolloid and Fluid Physics Group (ref. PAI-FQM115) of the University of Granada (Spain) and C. Moraila thanks to the University of Sinaloa (Mexico).

References

1 G. von Freymann, V. Kitaev, B. V. Lotsch and G. A. Ozin, *Chem. Soc. Rev.*, 2013, **42**, 2528–2554.
2 N. Vogel, C. K. Weiss and K. Landfester, *Soft Matter*, 2012, **8**, 4044–4061.
3 *Evaporative Self-Assembly of Ordered Complex Structures*, ed. Z. Lin, World Scientific, Singapore, 2012.
4 O. Kruglova, P.-J. Demeyer, K. Zhong, Y. Zhou and K. Clays, *Soft Matter*, 2013, **9**, 9072.
5 R. D. Deegan, O. Bakajin, T. F. Dupont, G. Huber, S. R. Nagel and T. A. Witten, *Nature*, 1997, **389**, 827–829.
6 L. Bocquet, *Am. J. Phys.*, 2007, **75**, 148–150.
7 H. Hu and R. G. Larson, *Langmuir*, 2005, **21**, 3963–3971.
8 T. A.H. Nguyen, A. V. Nguyen, M. a. Hampton, Z. P. Xu, L. Huang and V. Rudolph, *Chem. Eng. Sci*, 2012, **69**, 522–529.
9 G. Nägele, *Phys. Rep.*, 1996, **272**, 215 – 372.
10 S. S. L. Peppin, J. a. W. Elliott and M. G. Worster, *J. Fluid Mech.*, 2006, **554**, 147.
11 L. Daubersies and J.-B. Salmon, *Phys. Rev. E*, 2011, **84**, 031406.
12 A. Merlin, J. Angly, L. Daubersies, C. Madeira, S. Schöder, J. Leng and J.-B. Salmon, *Eur. Phys. J. E*, 2011, **34**, 1–7.
13 E. Widjaja and M. T. Harris, *AIChE J.*, 2008, **54**, 2250–2260.
14 L. Frastia, A. J. Archer and U. Thiele, *Phys. Rev. Lett.*, 2011, **106**, 077801.
15 K. A. Baldwin, M. Granjard, D. I. Willmer, K. Sefiane and D. J. Fairhurst, *Soft Matter*, 2011, **7**, 7819.
16 T.-S. Wong, T.-H. Chen, X. Shen and C.-M. Ho, *Anal. Chem.*, 2011, **83**, 1871–1873.
17 W. Sempels, R. De Dier, H. Mizuno, J. Hofkens and J. Vermant, *Nat. Commun.*, 2013, **4**, 1757.
18 S. Paddock and K. Eliceiri, *Confocal Microscopy*, Springer New York, 2014, vol. 1075, pp. 9–47.
19 I. Nikiforow, J. Adams, A. M. König, A. Langhoff, K. Pohl, A. Turshatov and D. Johannsmann, *Langmuir*, 2010, **26**, 13162–7.
20 F. J. M. Ruiz-Cabello, M. A. Rodríguez-Valverde and M. A. Cabrerizo-Vílchez, *J. Adhes. Sci. Technol.*, 2011, **25**, 2039–2049.
21 C. L. Moraila-Martinez, M. A. Cabrerizo-Vilchez and M. A. Rodriguez-Valverde, *Soft Matter*, 2013, **9**, 1664–1673.
22 C. A. Diaz, Y. Xia, M. Rubino, R. Auras, K. Jayaraman and J. Hotchkiss, *Nanoscale*, 2013, **5**, 164–8.
23 A. G. Marin, H. Gelderblom, D. Lohse and J. H. Snoeijer, *Phys. Fluids*, 2011, **23**, 091111–1.
24 D. Noguera-Marín, C. L. Moraila-Martínez, M. A. Cabrerizo-Vílchez and M. A. Rodríguez-Valverde, *Langmuir*, 2014, **30**, 7609–7614.

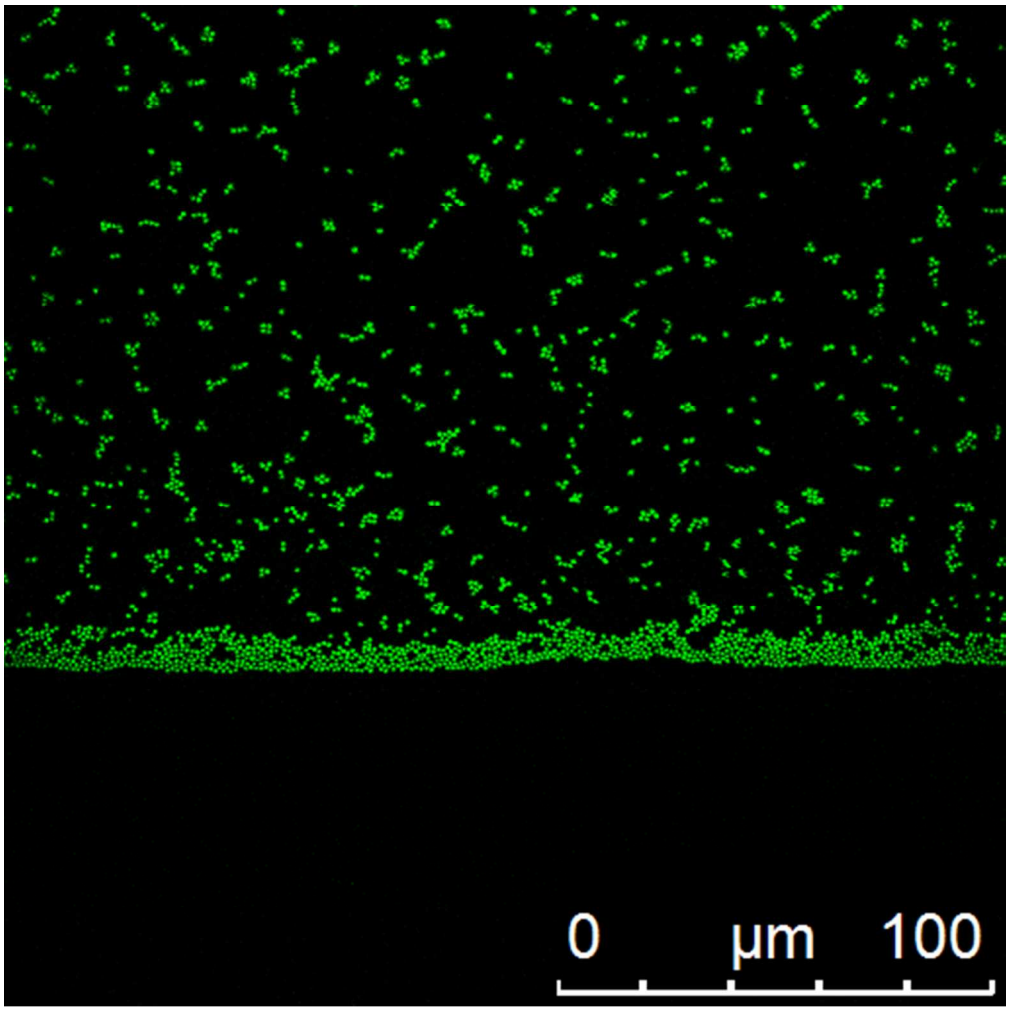

135x135mm (96 x 96 DPI)